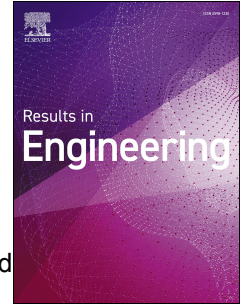


Journal Pre-proof

The impact of waste brick and geo-cement aggregates as sand replacement on the mechanical and durability properties of alkali-activated mortar composites

Eslam El-Seidy, Mehdi Chougan, Yazeed A. Ai-Noaimat, Mazen J. Al-Kheetan, Seyed Hamidreza Ghaffar



PII: S2590-1230(24)00050-1

DOI: <https://doi.org/10.1016/j.rineng.2024.101797>

Reference: RINENG 101797

To appear in: *Results in Engineering*

Received Date: 2 October 2023

Revised Date: 11 January 2024

Accepted Date: 12 January 2024

Please cite this article as: E. El-Seidy, M. Chougan, Y.A. Ai-Noaimat, M.J. Al-Kheetan, S.H. Ghaffar, The impact of waste brick and geo-cement aggregates as sand replacement on the mechanical and durability properties of alkali-activated mortar composites, *Results in Engineering* (2024), doi: <https://doi.org/10.1016/j.rineng.2024.101797>.

This is a PDF file of an article that has undergone enhancements after acceptance, such as the addition of a cover page and metadata, and formatting for readability, but it is not yet the definitive version of record. This version will undergo additional copyediting, typesetting and review before it is published in its final form, but we are providing this version to give early visibility of the article. Please note that, during the production process, errors may be discovered which could affect the content, and all legal disclaimers that apply to the journal pertain.

© 2024 Published by Elsevier B.V.

1 **The impact of waste brick and geo-cement aggregates as sand replacement**
2 **on the mechanical and durability properties of alkali-activated mortar**
3 **composites**

4 Eslam El-Seidy^a, Mehdi Chougan^a, Yazeed A. Al-Noaimat^a, Mazen J. Al-Kheetan^b, Seyed
5 Hamidreza Ghaffar^{a,c,d*}

6 ^a Department of Civil and Environmental Engineering, Brunel University, London, Uxbridge,
7 Middlesex, UB8 3PH, United Kingdom

8 ^b Department of Civil and Environmental Engineering, College of Engineering, Mutah
9 University Mutah, Karak 61710, P.O. BOX 7 Jordan

10 ^c Applied Science Research Center, Applied Science Private University, Jordan

11 ^d Department of Civil Engineering, University of Birmingham, Dubai International Academic
12 City, Dubai P.O. Box 341799, United Arab Emirates

13 *Corresponding author: seyed.ghaffar@brunel.ac.uk

14 **Highlights**

- 15 • Waste brick and geo-cement aggregates incorporated in Alkali Activated Materials.
- 16 • Waste brick and geo-cement aggregates established better compatibility with Alkali
17 Activated Materials.
- 18 • The highest compressive and flexural strengths were 61 and 12 MPa registered for
19 waste brick and geo-cement aggregates, respectively.
- 20 • Waste brick and geo-cement aggregates enhanced composites' durability.

21 **Abstract**

22 This study explores the potential of waste brick and geo-cement aggregates as substitutes for
23 natural sand in alkali-activated materials (AAMs) for mortar production. With a focus on
24 achieving net-zero construction and mitigating environmental impact, the study replaces
25 Portland Cement (OPC) and virgin aggregates with waste materials and by-products. The
26 investigation evaluates the substitution of sand (up to 100% by weight) in AAMs with waste
27 brick aggregates (WBA) and waste geo-cement aggregates (WGA) obtained from demolished
28 construction and research lab waste, respectively. The research methodology involves
29 assessing mechanical, durability, and microstructure properties to assess the performance of
30 the developed AAMs with waste aggregates. Notably, AAM composites containing waste brick
31 and geo-cement aggregates surpass natural aggregate composites in terms of mechanical
32 strength, water absorption, freeze-thaw resistance, acid ingress, and chloride attack. The 7-
33 day 50% waste brick mixture achieved a maximum compressive strength of 61 MPa, while a

34 70% waste geo-cement mortar mixture attained a maximum flexural strength of 12 MPa.
35 Combinations, whether comprising waste brick or geo-cement mortar aggregates,
36 demonstrate compressive strengths well over 40 MPa, rendering them suitable for heavy
37 load-bearing structures. The 50% waste geo-cement mortar mixture stands out with the
38 lowest water absorption rate of 6% and the least compressive strength loss of 13% after the
39 freeze-thaw test, with reductions of 6% and 18%, respectively, compared to the control.
40 Additionally, 100% waste brick AAMs exhibit the lowest compressive strength loss after
41 chloride and acid attack tests, with reductions of 13% and 2.5%, respectively. When compared
42 to all other mixtures, the 50% waste brick aggregates mortar mixture obtained the best
43 overall performance. The composites developed in this study affirm their suitability for use in
44 heavy-load structural components, showcasing favourable mechanical and durable
45 properties. These findings underscore the need for additional exploration in this direction to
46 advance sustainable construction practices

47 **Keywords**

48 Alkali-activated materials; waste brick; waste geo-cement; aggregates; durability

49 **1. Introduction**

50 Circular economy (CE) is an economic system that involves reducing, reusing, recycling, and
51 recovering materials throughout the production, distribution, and consumption of "end-of-
52 life" products [1]. Implementing CE strategies can help mitigate global warming and
53 environmental impacts caused by the construction industry, which is responsible for
54 approximately 36% of global carbon emissions, rising to 40-50% in industrialised countries [2].
55 Cement manufacturing, which is responsible for 8% of worldwide CO₂ emissions, significantly
56 contributes to the construction industry's environmental impact, producing approximately
57 2.083 billion tonnes of CO₂ annually. If the current rate of emissions is maintained, emissions
58 from the cement sector are expected to reach 2.34 billion tonnes annually in 2050 [3,4]. The
59 predicted CO₂ reductions in relation to AAMs and Portland cement ranged from 9% to 97%.
60 The exact alkali-activated binder mix design, the curing conditions used, the properties of the
61 reference Portland cement system, and geographical concerns connected to material
62 availability and transportation all affected these variances [5]. One of the perplexing issues
63 within the researchers studying alkali-activated binders revolves around the extensive spread
64 of various terms denoting essentially the same material. This nomenclature encompasses a

65 wide range of designations, including "alkali-bonded ceramic," "alkali ash material", "geo-
66 cement", "geopolymer", "hydro-ceramic", "inorganic polymer", "mineral polymer", "soil
67 cement", "soil silicate", among others [6]. The construction industry also consumes a large
68 percentage of natural resources, for instance, it consumes about 49% of raw stone, gravel,
69 and sand, 25% of virgin wood, and 16% of water [7]. As the demand for river sand in the
70 construction industry continues to grow, natural resources are being depleted and the
71 environment is being negatively affected, e.g. the decrease in the water table of rivers and
72 erosion of riverbanks [8]. Therefore, employing alternatives to cement and natural
73 aggregates, such as alkali-activated binders and construction and demolition waste (CDW), in
74 the concrete manufacturing sector is imperative, as they can significantly reduce CO₂
75 emissions while also improving mechanical and durability properties [9]. CDW is composed of
76 bulky and heavy materials such as concrete, wood, asphalt, gypsum, metals, bricks, glass,
77 plastics, soil, and rocks. Approximately 35% of the world's CDW is landfilled or illegally
78 disposed of, which poses significant environmental concerns and increases waste disposal
79 costs [10,11]. According to the US Environmental Protection Agency's advanced sustainable
80 materials management reports, 600 million tonnes of CDWs were created in the United States
81 in 2018. In 2016, the European Union (EU-28) generated 374 million tonnes of CDWs
82 (excluding excavated soil), the biggest waste stream (by mass)[12]. Moreover, bricks are the
83 second most frequently used building material after concrete, forming a significant portion of
84 the world's CDW. They are classified as Construction and Demolition (C&D) debris as they
85 sustain damage during the production, construction, or demolition processes [13]. Ground
86 clay brick is widely regarded as a pozzolanic material, where SiO₂, Al₂O₃, and Fe₂O₃ form over
87 70% of its constituents, satisfying the ASTM C618 criterion [13]. Brick masonry is used to
88 construct nearly all residential structures in the subtropical region, and 1391 billion bricks are
89 produced globally every year [14]. Moreover, each year, the European Union and the United
90 States produce roughly 800 and 700 million metric tonnes of CDW, respectively. China, the
91 world's largest developing nation, generates approximately 1.8 billion metric tonnes of
92 construction and demolition waste annually. Approximately 80% of the total CDW is
93 comprised of brick and concrete waste [15]. Additionally, M. Ngoc-Tra Lam et al. (2023) [16]
94 reported that about 54% of the CDW is composed of clay bricks and ceramic materials.
95 While the construction industry is still in the early stages of assessing the viability of
96 geopolymers, understanding the prospective challenges in dealing with geopolymers' waste

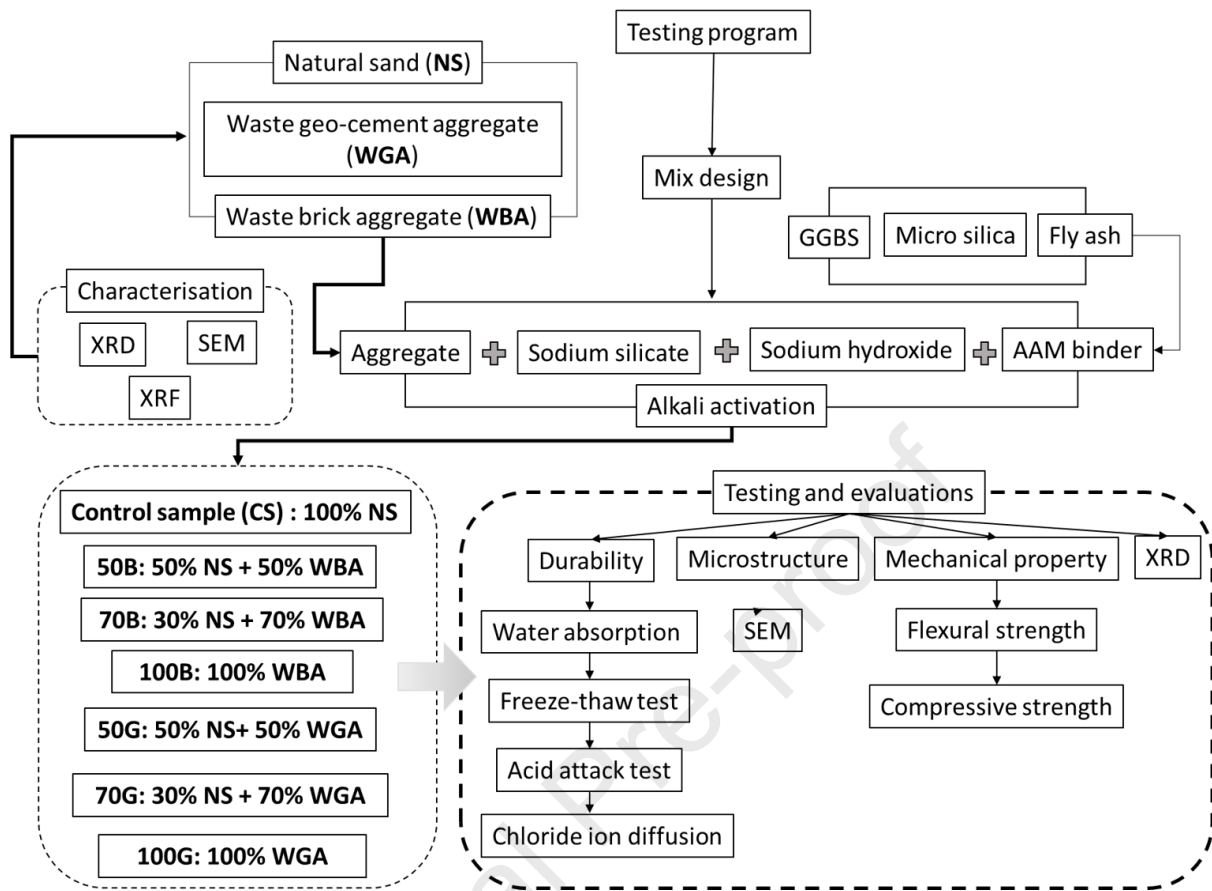
97 at the end-of-life of geopolymers concrete requires special attention [17]. Mesgari et al. [17]
98 assessed the use of geopolymer waste aggregates in geopolymer and OPC- based mixtures as
99 coarse aggregates with a size of 12 mm, where four replacement ratios were considered; 0,
100 20, 50, and 100% of the weight of natural coarse aggregates. They found that waste
101 geopolymer aggregates gave better results, at all replacement ratios, when incorporated in
102 the geopolymer concrete compared to OPC concrete in terms of mechanical properties. In
103 another study by Tavakoli et al. [18], natural sand in OPC-based concrete was replaced by
104 waste clay brick aggregates at five replacement ratios: 0, 25, 50, 75, and 100%. They indicated
105 that concrete with 25% waste clay brick aggregates obtained the highest compressive
106 strength of 43 MPa at 28 days, attributed to the waste clay brick aggregates' pozzolanic
107 activity, which enhances the bonding between aggregates and the paste. However,
108 incorporating waste clay brick aggregates in higher ratios than 25% was found to negatively
109 affect the strength of concrete due to the porous structure of waste clay brick aggregates and
110 the development of cracks. Atyia et al. [19] reached a similar conclusion that the inclusion of
111 high ratios of clay waste brick as fine or coarse aggregates in OPC-based composites
112 weakened their mechanical properties. This was attributed to the weaker nature of waste
113 clay aggregates and higher water absorption compared to natural aggregates. In a study
114 carried out by C. Wang et al. [20] to introduces fibre-reinforced recycled aggregate concrete
115 (FRAC) to address issues like low toughness and cracking in recycled aggregate concrete. By
116 incorporating steel fibre (SF) and polypropylene fibre (PPF) into the RAC matrix, the research
117 provides experimental results on FRAC's behaviour under cyclic compression, focusing on
118 damage growth and residual strain. The study proposes a constitutive model that accurately
119 predicts FRAC's performance, considering fibre content. The findings offer valuable insights
120 into enhancing the mechanical properties of recycled aggregate concrete, particularly in low
121 cycle loading scenarios. Moreover, C. Wang et al [21] conducted cyclic compressive tests on
122 various fibre-reinforced recycled aggregate concrete (FRAC) formulations, exploring their
123 hysteresis and damping properties. The study examined steel fibre (SF)-reinforced natural
124 aggregate concrete (SF-R-NAC), SF-reinforced RAC (SF-R-RAC), and polypropylene fibre (PPF)-
125 reinforced RAC (PPF-R-RAC) with different fibre contents. Key findings include the exploration
126 of residual strain development, a proposed modified stress–strain constitutive model, and an
127 analysis of FRAC's hysteretic characteristics, such as strain energy and viscous damping. The
128 study introduced a novel viscous damping model, accounting for fibre content, and validated

129 its effectiveness through predictions based on the modified constitutive model. C. Wang et
130 al.[22] studied the use of a dynamic constitutive model for recycled aggregate concrete (RAC)
131 to analyse the impact of strain rate and replacement ratio on structural restoring force
132 behaviours, focusing on recycled coarse aggregate (RCA). It introduces a rate-dependent
133 damage model for RAC frame structures and provides calculation models for characteristic
134 parameters and strain rate influence factor models for various structural behaviours.
135 The principle of this research is to embrace circular economy strategies in cementitious
136 composite production by exploring the potential of utilising waste brick and geo-cement as
137 fine aggregates in alkali-activated formulations. Natural sand was replaced by waste materials
138 in four replacement ratios of 0, 50, 70, and 100%, and composites' mechanical, physical,
139 microstructure, and durability properties were investigated to understand the behaviour of
140 recycled aggregates and potential opportunity for reserving natural sand in cementitious
141 composites. To the best of the authors' knowledge, this is the first research to incorporate
142 waste brick and cement-free geo-cement mortar to completely replace natural sand
143 aggregates in alkali-activated cementitious composites and to assess various durability tests.
144 Despite the considerable number of studies conducted on the topic, there is a shortage of
145 research specifically focused on geo-cement aggregates used in alkali-activated materials.
146 Furthermore, there is a scarcity of studies that have fully (i.e., 100%) replaced natural sand
147 with waste brick and waste geo-cement aggregates in AAM systems. Our approach, which
148 involves the development of low-carbon composites featuring zero cement and zero natural
149 sand, while being suitable for a load-bearing structure and substantial durability, represents
150 a groundbreaking step towards the implementation of a net-zero strategy.

151 **2. Experimental framework**

152 Figure 1 explains the experimental methodology and characterisation procedures used in this
153 study to explore the performance of low-carbon cementitious composites using waste
154 aggregate replacements in detail.

155

156 **Figure 1.** The experimental design of the study157 **2.1. Materials**

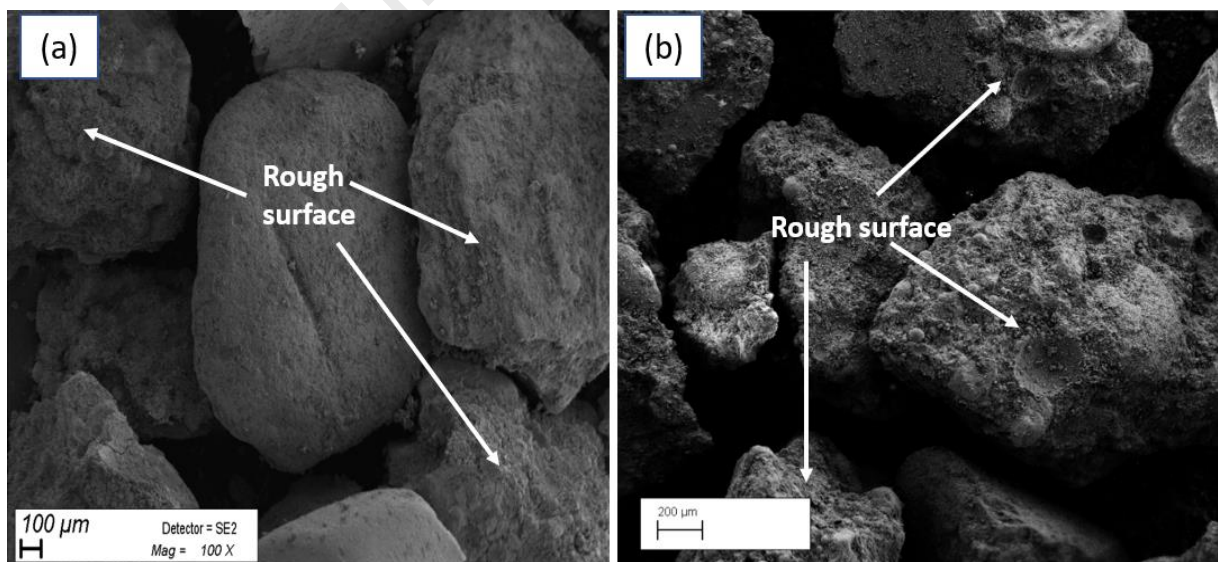
158 The alkali-activated cementitious composites were prepared using (1) fly ash (FA) (Cemex,
 159 UK); (2) granulated blast furnace slag (GGBS) (Hanson Heidelberg Cement, UK) that abides
 160 with EN 15167-1; (3) micro-silica (MS) (J. Stoddard & Sons Ltd); (4) graded sand including two
 161 distinct sand sizes of 0–0.5 mm and 0.5–1.0 mm in accordance with BS EN 410–1:2000; (5)
 162 sodium silicate (Na_2SiO_3) solution with the $\text{SiO}_2/\text{Na}_2\text{O}$ mass ratio of 3.0 (Solvay SA, Portugal);
 163 (6) 10 mol/l sodium hydroxide (NaOH) solution (Fisher Scientific, Germany); and (7)
 164 attapulgite nano clay additive with a fixed dose of 1% by weight of binder (based on authors'
 165 prior research) [23]. The mix formulation has been developed by the authors from previous
 166 works based on several trials and errors [24,25]. Two type of waste aggregates were studied
 167 in this investigation, namely, waste brick aggregates (WBA) and waste geo-cement aggregates
 168 (WGA). Waste bricks were picked up from a demolished building on the Brunel University
 169 campus, cleaned and then manually broken into chunks and ground to a size of 1-2 mm using
 170 Retsch SM100 electric grinder. The waste geo-cement was collected from the cast specimens
 171 in the civil engineering laboratory at Brunel University. These geo-cements were cured at 60

172 °C for 24 hours, left at room temperature for 6 days for testing in another research. The waste
 173 of these specimen was then manually broken down into smaller pieces, and then ground using
 174 the lab grinder to a size of 1-2 mm. The size of the aggregates was established by considering
 175 two factors: (1) the size of the local grinder's sieves and (2) minimizing energy consumption
 176 during the grinding process for finer aggregates. **Figure 2** illustrates the aggregates'
 177 microstructure and rough surface textures of (a) the waste brick aggregates consist of a
 178 combination of rounded and sharp-edged particles, while (b) the waste geo-cement
 179 aggregates exhibit angular edges with scattered notches on the surface. Table 1 illustrates the
 180 chemical composition of WBA and WGA. As shown in **Figure 4**, several phases (i.e., Quartz
 181 (Q), Muscovite (MS), Carbon (C)) in both brick and geo-cement aggregates used in this study
 182 have been identified using XRD.

183 Table 1. The chemical compositions of the WBA and WGA by X-ray fluorescence (XRF)

Material	SiO ₂ (Wt.%)	CaCO ₃ (Wt.%)	Al ₂ O ₃ (Wt.%)	Fe ₂ O ₃ (Wt.%)	P ₂ O ₅ (Wt.%)	K ₂ O (Wt.%)
Waste brick aggregates (WBA)	74	0.761	12.7	6.56	2.69	1.79
Waste geo-cement aggregates (WGA)	52.6	15.4	9.65	4.91	2.86	1.2

184 The high quantity of CaCO₃ in WGA is due to the possibility of the reaction of the CO₂ of the
 185 surrounding environment with the Cao of the GGBS[6].



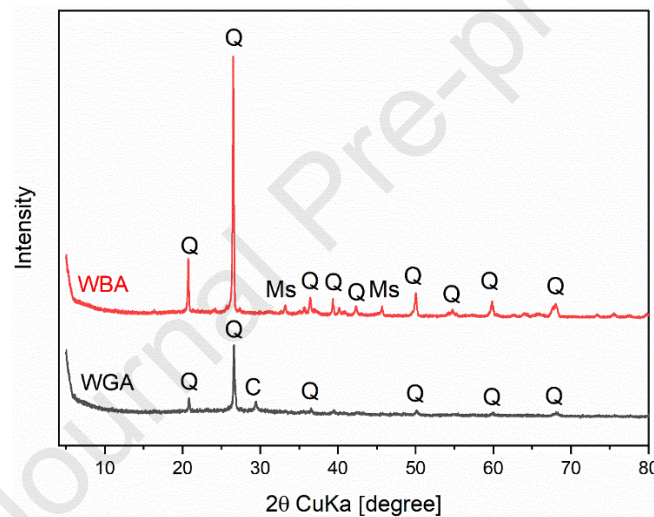
186
 187

Figure 2. Microstructure of (a) waste brick aggregates and (b) waste geo-cement aggregates



188

189 **Figure 3.** The process of obtaining WBA and WGA (a) chunks of bricks, (b) chunks of geo-
 190 cement, (c) The grinding machine, (d) grinding cylinder, (e) waste break aggregates, and (f)
 191 geo-cement aggregates



192

193 **Figure 4.** XRD patterns of (a) waste brick aggregates and (b) waste geo-cement aggregates

194 **2.2. Mix formulation and material preparations**

195 A total of seven AAM mixes were prepared. The formulation of the control AAM mix (control
 196 sample - CS) detailed in Table 2, was chosen based on the authors' past research [23]. The
 197 chemical characterizations of the binders have been detailed in a prior publication by the
 198 authors. [26]. At the outset, the precursor materials, which included FA, GGBS, SF, and
 199 aggregates (graded sand, WBA, and WGA), were dry mixed for 5 minutes at 250 rpm using a
 200 planetary mixer (Kenwood, Germany), maintaining a consistent binder-to-aggregates ratio of
 201 0.8. In this study, 50 wt.-%, 70 wt.-%, and 100 wt.-% of natural sand aggregates was replaced
 202 with recycled aggregates (i.e., WBA and WGA). The establishment of replacement ratios is
 203 grounded in our prior research, wherein waste plastic aggregates (UPVC) were replaced up to
 204 100% [27]. Despite the inherent drawbacks associated with using plastic aggregate, we

205 successfully attained commendable mechanical properties. Subsequently, this scientific
 206 groundwork provided the rationale to extend our investigation to mineral aggregates such as
 207 WGA (waste geo-cement aggregates) and WBA (waste brick aggregates) for complete
 208 substitution in lieu of sand. The alkali activator solutions (i.e., a mixture of 10 mol/l NaOH and
 209 Na_2SiO_3 with the $\text{SiO}_2/\text{Na}_2\text{O}$ weight ratio of 3.23 and molar ratio of 3.3-3.5) with a mass ratio
 210 of 1:2 were mixed for 5 minutes using a magnetic stirrer, w/b ratio was 0.4 for all mixes.
 211 Finally, premixed alkali solutions were added gradually to the dry mixture, then mixed for 10
 212 minutes at 450 revolutions per minute until homogenous AAM mixes with normal consistency
 213 and easy to spread and work with while maintaining proper cohesion, were obtained to
 214 produce mortar. AAM fresh mixes were cast using prismatic moulds with dimensions of 160
 215 x 40 x 40 mm³ for mechanical tests and metal cube moulds with dimensions of 50 x 50 x 50
 216 mm³ for durability tests (three samples for each mix) and put in an oven for 24 hours at 60 °C
 217 (heat curing stage) followed by 6 days (air curing stage) at ambient temperature.

218 Table 2. Mix formulation for AAM mixtures with waste brick aggregates (WBA) and waste
 219 geo-cement aggregates (WGA) at different replacement ratios

Sample ID	Binder (wt.%)			Aggregate (wt.%)			
	FA	GGBS	Micro silica	Natural sand		Recycled aggregate	
				0 - 0.5 mm	0.5 - 1 mm	WBA	WGA
CS	60	25	15	60	40	0	0
50B	60	25	15	30	20	50	0
70B	60	25	15	18	12	70	0
100B	60	25	15	0	0	100	0
50G	60	25	15	30	20	0	50
70G	60	25	15	18	12	0	70
100G	60	25	15	0	0	0	100

220

221 2.3. Experimental tests

222 2.3.1. Microstructure analysis

223 Microstructural analysis of alkali-activated materials (AAMs) was conducted utilising scanning
 224 electron microscopy (SEM) with a Supra 35VP instrument from Carl Zeiss, Germany. Each
 225 composition underwent analysis through at least ten samples, each measuring 8 mm³ in size.
 226 Prior to SEM examination, all samples were subjected to gold coating using an Edwards S150B
 227 sputter coater to enhance electrical conductivity.

228 2.3.2. Mechanical properties

229 The mechanical performance of AAM samples (i.e., flexural, and compressive strengths) was
230 assessed after 7 days of curing in accordance with BS EN 196-1:2016, using an Instron 5960
231 Series Universal Testing System. For each composite, three samples were tested for flexural
232 strength and six samples for compressive strength. The loading rate was adjusted at 1
233 mm/min for both flexural and compressive tests in accordance with BS EN 196-1:2016.

234 **2.3.3. Freeze-thaw test**

235 Three cubes with the size of 50 x 50 x 50 mm³ for each composite were frozen in cold air and
236 thawed in water following the procedure of ASTM C666/C666M. Freezing and thawing (F–T)
237 temperatures were -20 °C and 20 ± 2 °C, respectively. Both the freezing and thawing
238 timeframes were set to 12 hours, indicating a single F–T cycle. In addition, the number of F–
239 T cycles is 50. The degradation of the composites' mechanical characteristics due to F–T cycles
240 was then examined in terms of mass loss and loss of compressive strength. Equations 1 and 2
241 were used to calculate the mass and the compressive loss.

242 **2.3.4. Chloride attack test**

243 This test was performed by immersing composites' samples in a saline solution, as per ASTM
244 D114198. The samples with the dimensions of 50 x 50 x 50 mm³ were immersed in tap water
245 with 5% sodium chloride for six weeks. Afterwards, all samples were dried, Subsequently, an
246 analysis of the deterioration in the mechanical properties of the composite due to chloride
247 penetration was conducted, focusing on the loss of compressive strength. the compressive
248 strength loss was calculated followed the formula below:

$$249 \text{ Compressive strenght loss \%} = \frac{\text{Initial compressive strength} - \text{Final comperssive strength}}{\text{Initial compressive strength}} \times 100 \quad (\text{Equ.1})$$

250 Where, initial compressive strength is the compressive strength of a composites (MPa) after
251 7 days of curing, and the final compressive strength is the compressive strength of a
252 composite (MPa) after conducted the Chloride test.

253 **2.3.5. Acid attack test**

254 The acid resistance of the cementitious samples with the dimensions of 50 x 50 x 50 mm³ was
255 assessed by exposing them to an acidic solution for 28 days. In line with ASTM C189820, the
256 acidic solution was created by dissolving 5% sulphuric acid in 40 litres of tap water. After 28
257 days, the specimens were dried and weighed. The impact of acid attack on the mechanical
258 properties of the composite was further examined, specifically in terms of weight loss and the
259 reduction in compressive strength. the weight loss was calculated following the equation
260 below:

$$261 \quad \text{Weight loss \%} = \frac{\text{Initial Weight} - \text{Final Weight}}{\text{Initial Weight}} \times 100 \quad (\text{Equ.2})$$

262 Where, Initial weight is the composite's weight before the test (g), and final weight is the
 263 composite's weight after performing the acid attack test (g). To calculate the compressive
 264 strength loss, Equation 1 was applied.

265 **2.3.6. Water absorption test for the composites**

266 The conventional weight-measuring method following the ASTM C1585-13 procedure was
 267 used to assess the capillary water absorption of the composites. Each mixture was evaluated
 268 using a batch of three cubes, each measuring 50 x 50 x 50 mm³. The specimens were placed
 269 in an oven at (60 ± 5 °C) until completely dry, after which the water absorption was measured
 270 at regular intervals over an eight-day period. Finally, the capillary water absorption rate of
 271 the composites was determined using the following formula:

$$272 \quad \text{Water absorption (\%)} = \frac{M_t - M_0}{M_0} \times 100 \quad (\text{Equ.3})$$

273 Where, M₀ (g) represents the oven-dried mass, and M_t (g) represents the saturated surface-
 274 dry mass.

275 **2.3.7. Water absorption test for the aggregates**

276 Water absorption (WA) is calculated as the ratio of the water needed to saturate a porous
 277 sample to its dry mass. The measurement involves drying the samples at a specified drying
 278 temperature (20°C; 30°C; 45°C; 75°C; 105°C) to eliminate all water present in the pores (M_{dry}).
 279 Subsequently, the samples are immersed in water using a solid-to-liquid ratio of 100g to 1 L.
 280 The immersion is static, and the dissolution of the aggregates is considered slow, rendering
 281 leaching negligible [28]. After 24 hours of water immersion, the samples are taken out of the
 282 water. Finally, the aggregate surface is meticulously dried with absorbent cloths until the
 283 water films on the aggregate surface vanish, achieving the "Saturated Surface Dry" (SSD) mass
 284 (M_{SSD}) in accordance with standard NF EN 1097-6 [29]. From these two measurements, the
 285 water absorption is calculated as:

$$286 \quad \text{Water absorption (\%)} = \frac{M_{SSD} - M_{dry}}{M_{dry}} \times 100 \quad (\text{Equ. 4})$$

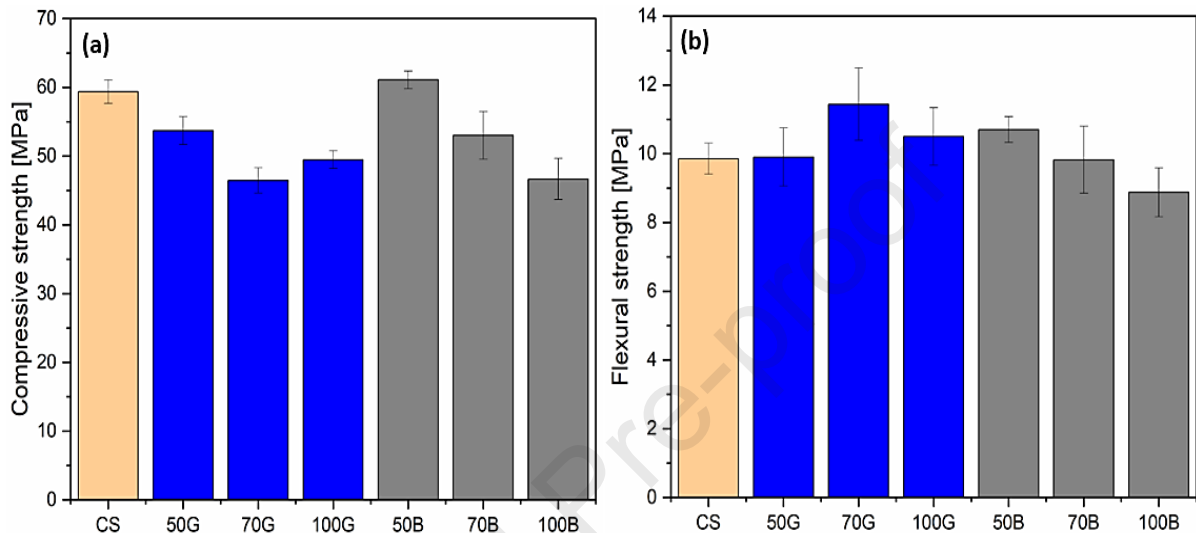
287 **3. Results and Discussion**

288 **3.1. Mechanical characteristics**

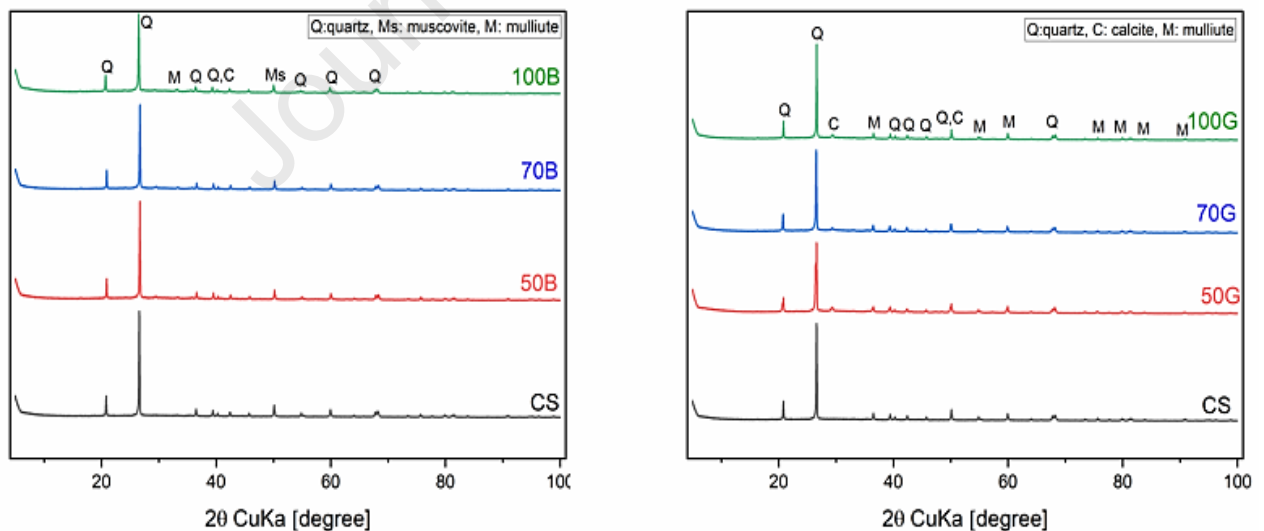
289 **Figure 5** displays the compressive and flexural strength results of AAM composites containing
 290 waste geo-cement and waste brick aggregates. It is evident that there are changes in the

291 compressive and flexural strength of the specimen with recycled aggregates compared to the
292 control sample. As shown in **Figure 5 a**, the compressive strength values after incorporating
293 WGA aggregates were reduced compared to the CS. The highest reduction of 23% was
294 obtained by the 70G sample. However, increasing the aggregate replacement percentages
295 followed a reverse trend for flexural strength values. In a study conducted by Zhu et al. [30],
296 the inclusion of more than 50% recycled geopolymer aggregate in the metakaolin-based
297 geopolymer system resulted in a noticeable reduction in flexural and compressive strengths.
298 Their results indicated that the reduction in compressive strength is associated with increased
299 porosity of the composites, which is induced by the water absorption of the geopolymer
300 aggregates, i.e., less available water in the system. However, the mechanical performance
301 reduction rate is relatively milder than incorporating recycled mortar aggregates in a OPC-
302 based cementitious system [30,31]. Compared to the value recorded for the control sample
303 (i.e., 10 MPa), the flexural strength values first remained constant for 50G, then increased,
304 and reached 12 MPa and 11MPa for the 70G and 100G samples, respectively. The maximum
305 flexural strength was about 12 MPa obtained for the 70G mixture, which was about 20%
306 higher than the CS. The modest increase in flexural strength in comparison to CS may be
307 attributed to the bridging effect induced by WBA and WGA, thereby augmenting the flexural
308 strength of the composites. This proposition finds support in a study conducted by G.
309 Hauseien et al. [30], where ceramic waste powder from tiles (TCW) was integrated into alkali-
310 activated composites utilising fly ash and ground granulated blast furnace slag (GGBS). The
311 researchers noted that incorporating a substantial concentration of TCW led to minimal
312 cracking, ascribed to the bridging effect of TCWs. This phenomenon heightened the capacity
313 for energy absorption, mitigating the risk of sudden failure or collapse in the specimens.
314 Another reason might be due to that WBA are driven from burnt clay bricks and then
315 pulverised. The conventional brick kiln undergoes heating up to 1000–1500 °C, causing
316 alumina, silica, and iron to transform into fused glass, serving as a binding agent for adhesion
317 [32]. This stability leads to a stronger and more robust structure, providing the composites
318 integrated with WBA with consistently superior mechanical behaviour compared to those
319 with WGA. Conversely, WGA did not undergo exposure to such extreme temperatures,
320 preventing the development of strong adherence in the WBA structure. It is likely that the
321 weaker structure of WGA experienced a somewhat inconsistent reaction during alkalisation,
322 resulting in inconsistent mechanical behaviour.

323 The results indicated no obvious trend among composites containing WGA, on the other
 324 hand, composites containing WBA showed a declining of mechanical properties with the
 325 increasing of replacement ratios. For samples containing WBA, their compressive and flexural
 326 strengths slightly increased from 60 MPa and 10 MPa for CS and reached 61 MPa and 11 MPa
 327 for 50B. Subsequently, the compressive and flexural strengths gradually decreased to 52 MPa
 328 and 10 MPa for 70B and 45 MPa and 8 MPa for 100B, respectively.



329
 330 **Figure 5.** (a) Compressive strength and (b) Flexural strength of the AAM composites with
 331 waste geo-cement (G) and waste brick (B) aggregates

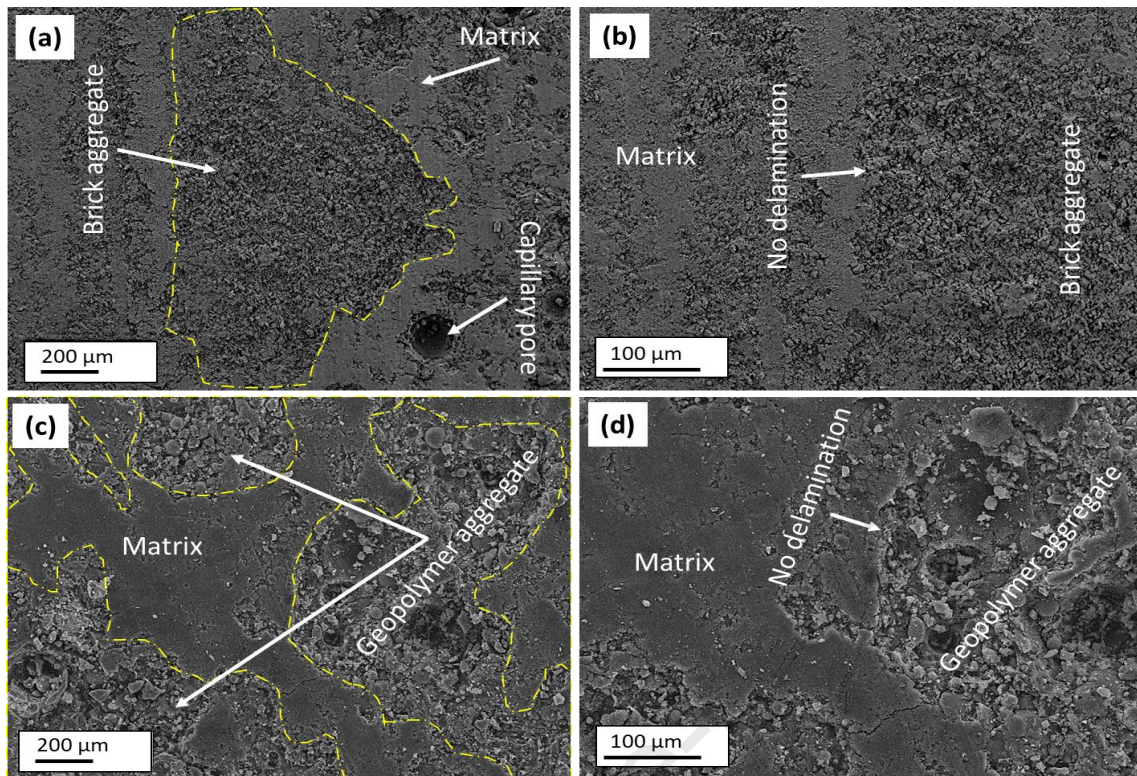


332
 333 **Figure 6.** XRD patterns of the AAM composites with (a) waste brick and (b) waste geo-
 334 cement aggregates

335 The findings of this study align with the research conducted by Khattab et al. [33], which
 336 investigated the substitution of waste brick aggregates for natural aggregates in a Portland
 337 cement-based mortar. In both studies, a complete replacement of natural sand led to a

338 decrease in compressive strength, amounting to a 22% reduction. This decline was ascribed
339 to the heightened porosity observed in the structure of the mortar. The compatibility
340 between WBA and WGA aggregates and the binder was confirmed by examining the
341 composites' microstructure (**Fig. 7 (a and b) and (c and d)**). **Fig. 2** also verified the obtained
342 results by revealing that both aggregates utilised in this investigation have comparable rough
343 surface textures, which played a crucial role in aggregate and cement paste interlocking
344 bonds. The rough surfaces and similar shapes of the waste aggregates to natural aggregate
345 facilitated the bonding between waste aggregates and the mortar, leading to a cohesive
346 composite with dense microstructure.

347 Regarding WBA, Olofinnade et al. [34] stated that based on the chemical composition of clay
348 brick aggregate and in accordance with the ASTM C618 standard for pozzolanic materials, the
349 material can be categorised as a class N pozzolan material. Recycled crushed brick aggregates
350 can be used to reduce dead loads, efflorescence, and maintain good shape without
351 maintenance, as well as reduce the cost of concrete. Crushed brick aggregates decrease the
352 compressive and tensile strengths of concrete while increasing the compressive strength of
353 mortar [35]. In a research conducted by P. Shewale et al. [36] to substitute natural sand with
354 waste brick at 10%, 20%, and 30% replacement ratios in fly ash and GGBS-based mortar, they
355 found that the incorporation of waste brick aggregates reduced the compressive strength of
356 the composites. Moreover, Khalil et al. [37] conducted a study to evaluate the use of brick
357 aggregates to substitute natural sand at 10%, 20%, and 30% ratios in geopolymer mortar
358 based on metakaolin. They reported that an increase in brick aggregates lowered compressive
359 strength, which can be attributable to the aggregate's lower strength and hardness compared
360 to natural aggregates. Based on the research conducted by Hu et al. [31], the addition of
361 recycled aggregate in fly ash/GGBS geopolymers had minimal impact on the mechanical
362 performance of the mixture, even with increasing replacement ratios from 50% to 100%. Their
363 study affirmed that the microstructure of the geopolymer matrix and the morphology of the
364 matrix/aggregate interface remained largely unchanged after substituting natural aggregate
365 with recycled aggregates. However, it was observed that the utilization of recycled aggregate
366 resulted in a slight reduction in mechanical properties, primarily attributable to the higher
367 presence of defects in recycled aggregates compared to natural counterparts.



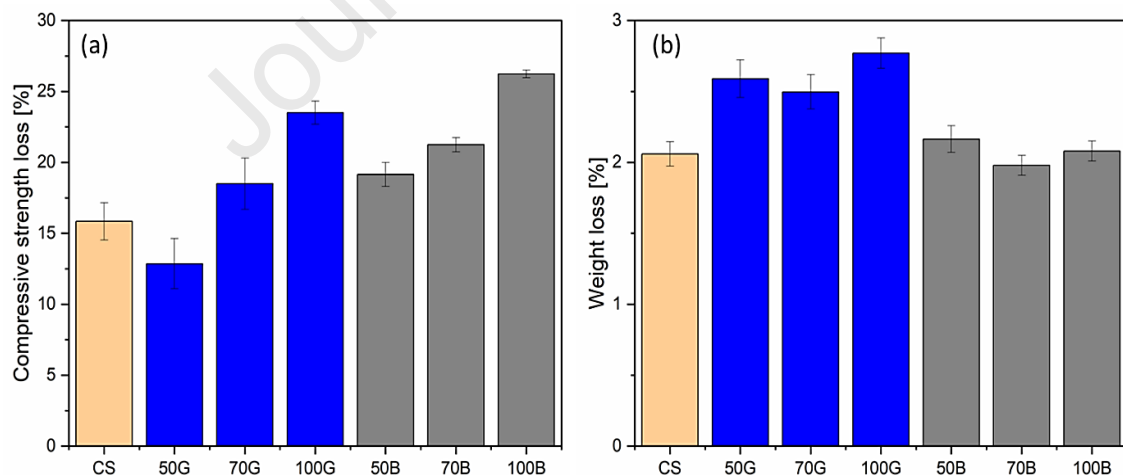
368 **Figure 7.** Microstructure of (a) and (b) AAM composite with WBA, and (c) and (d) AAM
 369 composite with WGA.
 370

371 **3.2. Durability properties**

372 **3.2.1. Freeze-thaw assessment**

373 The freeze-thaw (F-T) failure of a concrete structure occurs in three stages: water penetration,
 374 freezing, and structural collapses. At the stage of water absorption, external water enters the
 375 concrete through microcracks and fills the interior pores to near saturation. When the
 376 ambient temperature decreases to sub-zero degrees, the volume of frozen water swells by
 377 9%, and the inner wall of water-saturated pores undergoes tensile stress, leading to cracks
 378 and cement matrix spalling [38]. **Figure 8a-b** illustrates the compressive strength and weight
 379 loss, following the 50 F-T cycles, the composites were weighed, and their compressive
 380 strengths were calculated and compared. As predicted, the weight and compressive strength
 381 of each composite decreased. 50G exhibited the lowest drop in compressive strength, by
 382 about 13%, while 100B had the highest reduction, around 26%. Control sample's compressive
 383 strength dropped by about 16%. The compressive strength of 70G and 50B decreased by
 384 approximately 17%, followed by 70B and 100G, which decreased by 21% and 23%,
 385 respectively (see **Fig. 8-a**). The weight loss of the investigated composites ranges from 2% to
 386 3%, indicating their remarkable resistance to extreme temperature conditions (see Fig. 7-b).
 387 Notably, the compressive strength of composite 100B was measured at 33 MPa following the

388 50 F-T cycles, and it exhibited the highest compressive strength loss (26%). This outcome
 389 provides further evidence of the composites' ability to function effectively in hostile
 390 environments. Regarding compressive strength loss, composites containing WGA performed
 391 better than those containing WBA across all replacement ratios. However, in terms of weight
 392 reduction, no clear pattern was observed among the composites. It's worth noting that brick
 393 made from pulverized clay is commonly considered a pozzolanic material. Pozzolans, when
 394 combined with water, interact with calcium hydroxide, resulting in the production of (CSH)
 395 and (CASH). This interaction enhances the properties of cement-based structures, providing
 396 further advantages to these composites [13,39]. Rheological characteristics of geopolymer
 397 are proportional to activator concentration and Si/Na molar ratio, and yield stress and
 398 viscosity will rise when increased. The extremely high ratio has the opposite effect, dissolving
 399 ions that are too late to react and preventing the creation of a network [40]. Subsequently,
 400 composites containing WBA and WGA undergo reaction, which may result in a high ratio of
 401 Si/Na has the opposite effect, scattering ions that are too slow to react and suppressing
 402 network development. Since various interacting characteristics influenced the matrix
 403 structures, it was difficult to comprehend the behaviour of composites when subjected to F-
 404 T cycles. In addition, to the best of the author's knowledge, no research has been conducted
 405 on WGA and WBA in AAM composites subjected to the freeze-thaw test.



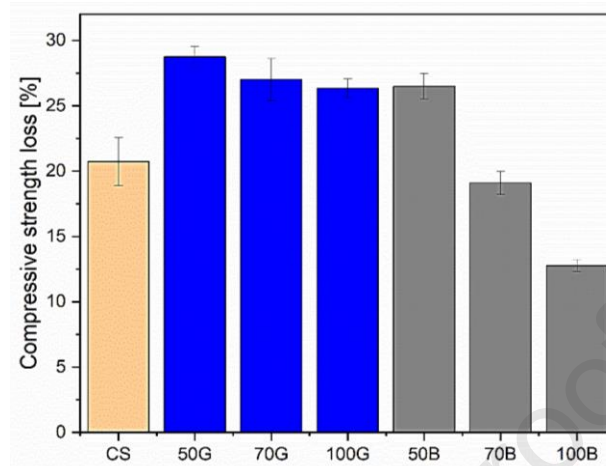
406
407 **Figure 8.** (a) Compressive strength loss % and (b) weight loss % after freeze- thaw test

408 3.2.2. Chloride attack assessment

409 The chloride attack on reinforced concrete is perhaps the most often seen and studied aspect
 410 of concrete's endurance. Through capillary absorption, hydrostatic pressure, and/or ion
 411 diffusion, chlorides are capable of penetrating. Chlorides stimulate the corrosion of
 412 embedded steel bars through a de-passivation process, resulting in a loss in the concrete's

413 load-bearing capacity and possibly its structural collapse. Moreover, The predominant alkali-
414 activation reaction products, namely C–A–S–H and N–A–S–H binding gels, which regulate
415 ionic transport processes, have an effect on the chemistry and transport mechanisms of
416 chloride in geopolymer mortar [41]. **Fig. 9** depicts the reduction in compressive strength of
417 composites after the execution of the chloride attack test. 100B had the lowest compressive
418 strength loss of around 13%, whereas 50G had the highest of approximately 28%, while
419 control sample's (CS) strength loss was 21%. 100B outperformed CS by 62%, while 50G trailed
420 behind by 33%. 70B exhibited the second-lowest compressive loss, at 17%, which is superior
421 to CS by 19%. The compressive strength loss of 70G, 100G, and 50B was around 26%, which
422 was 24% less than that of CS. Raising the replacement ratio of natural sand with WBA
423 significantly improved the chloride ingress resistance of the composite, whereas WGA had
424 the reverse effect. Since WGA aggregates consist of fly ash, slag, and silica sand, which already
425 reacted with alkali activators. The rheological properties of geopolymers are proportional to
426 the alkali activator concentration and Si/Na molar ratio. If done correctly, increasing the Si/Na
427 molar ratio could increase the rate of dissolution and polymerisation, leading to a rise in the
428 yield stress and viscosity of geopolymers. Nevertheless, the super-high ratio has the
429 contrasting effect, possibly because many ions that are late to react are dissolved, and their
430 repulsion inhibits network formation [40] and this may have worked in favour of chloride ions
431 penetration. On the other hand, the pozzolanic WBA had a significant impact on reducing the
432 chloride ingress and eventually, minimising compressive strength loss. These findings are
433 supported by a few studies on Portland cement-based composites, which stated that the
434 chloride content profiles reveal that concrete samples containing pozzolans had a
435 considerably reduced chloride content at various periods and depths, particularly in deeper
436 zones [42–44]. Moreover, the favourable effect the pozzolanic reaction of this pozzolan and,
437 as a result, the consumption of calcium hydroxide, which results in an increase in tortuosity
438 and a decrease in OH⁻ in the pore solution. As a result, chloride ion conductivity and chloride
439 penetration diminish [45]. This study revealed that composites containing 100B exhibited
440 remarkable resistance to chloride penetration. Alkali-activated materials (AAMs) generally
441 display lower chloride permeability compared to Portland/blend cements. However, there is
442 currently no comprehensive database of chloride diffusion coefficients for AAMs. This
443 discrepancy can be attributed to the fact that AAMs have been studied more extensively by
444 materials scientists than by concrete technologists. Consequently, there remain unanswered

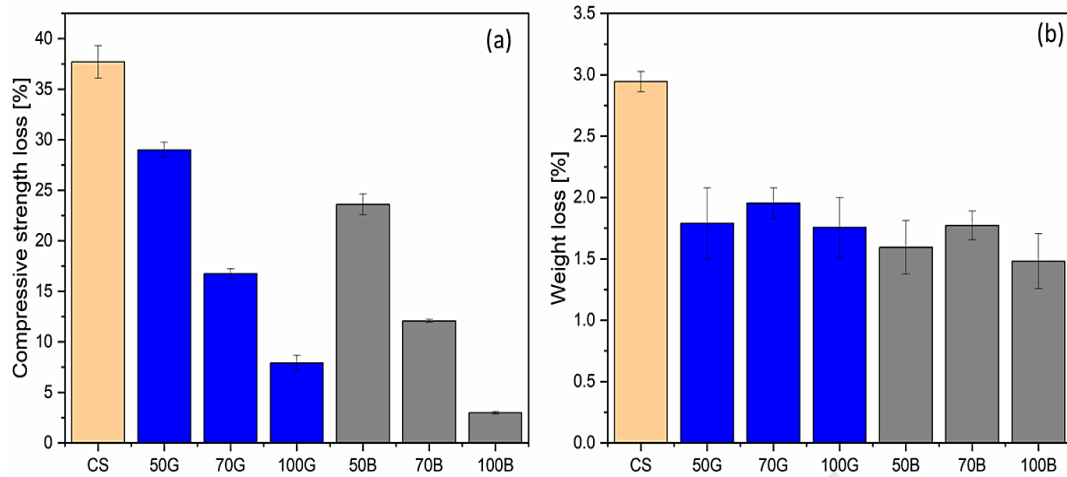
445 questions regarding the accurate determination of these coefficients for non-Portland
 446 cements. This critical issue necessitates the attention and collaborative efforts of the scientific
 447 community to address and resolve [6].



448 **Figure 9.** Compressive strength loss % after chloride attack test
 449

450 3.2.3. Acid attack assessment

451 Acids in groundwater, chemical wastewater, or acids coming from the oxidation of sulphur
 452 compounds in backfill can attack and affect the durability of concrete substructure
 453 components. In addition, various concrete structures are vulnerable to acid rain erosion,
 454 particularly in industrial districts where sulphuric acid is frequently prevalent. Moreover,
 455 sulfuric acid corrodes sewer pipelines and waste treatment plants [46]. As illustrated in the
 456 outcomes presented in **Figure 10**, both composites incorporating waste-derived aggregates
 457 exhibited superior performance compared to the control (refer to **Fig. 10-a**) in terms of
 458 compressive strength reduction. The incorporation of both WBA and WGA enhanced
 459 composites' acid attack resistivity. With the increase in incorporation aggregates, the loss of
 460 compressive strength decreased. Samples containing WBA performed better than samples
 461 containing WGA across every single replacement ratio in terms of compressive strength loss.
 462 100B had the lowest drop in compressive strength, of around 2.5%, while CS had the most,
 463 of approximately 37%. 70B had the second-lowest reduction in compressive strength of about
 464 12%, followed by 50B of about 23%. On the other hand, 50G, 70G, and 100G recorded
 465 compressive strength losses of about 28%, 17%, and 7%, respectively. 100B was 93% better
 466 than the control, while 50G was 24% better in terms of comprehensive strength loss.



467
468 **Figure 10.** (a) compressive strength loss % and (b) weight loss % after acid attack test

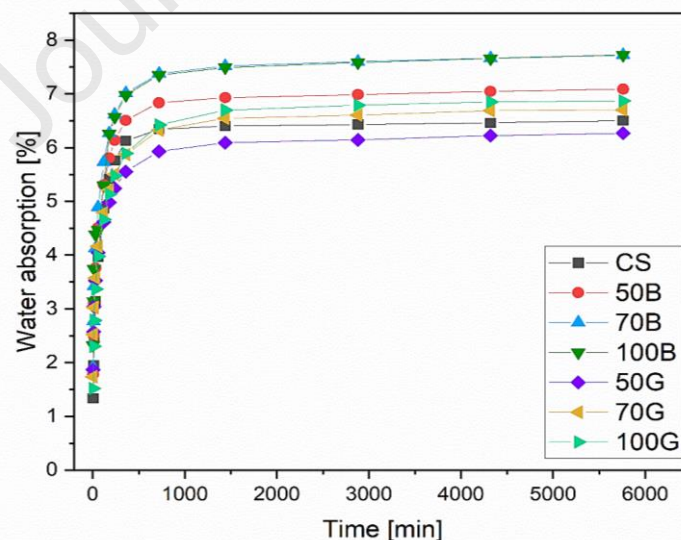
469 **Fig.10-b** illustrated the composites' weight loss after performing the acid attack test. All
 470 samples containing WBA or WGA had a weight loss of less than 2%, illustrating the composites
 471 strength against acid attack. On the contrary, the control's weight loss was about 3%, which
 472 is higher than the rest of the composites and indicated that the loss was significant as it
 473 dropped the control's compressive strength by 37%. In a study carried out by Izzat et.al (2013)
 474 [47] to examine OPC and geopolymer mortars, they stated that both mortars were shown to
 475 be susceptible to acidic attacks. The weight changes and the decrease in strength are
 476 consistent with this notion. Nevertheless, they affirmed that geopolymer specimens exhibited
 477 reduced susceptibility to acidic attack, as evidenced by weight changes and strength
 478 reductions of 3.6% and 24%, respectively. In contrast, OPC-based specimens experienced
 479 higher vulnerability with values of 18% and 69% for weight changes and strength reductions,
 480 respectively. It was proven that the durability performance of red clay brick
 481 waste/phosphorus slag-based geopolymer is related to its comparatively low calcium
 482 concentration and its extremely acid-resistant aluminosilicate composition. Moreover, acid
 483 attack resulted in significant calcium and sodium leaching into the acid solution,
 484 demonstrating the weak chemical link between calcium and sodium cations in the paste
 485 matrix. Existing unreacted brick particles in the matrix contribute to the low sodium content
 486 of the material, which is resistant to acid attack and exhibits a strong bonding type [48].
 487 In a study carried out by Nuaklong et. al [49] where two types of fly ash were used, one with
 488 low calcium content and the other with high calcium content. They confirmed that a
 489 geopolymer-based substance with a low calcium content was less susceptible to degradation
 490 by a sulfuric acid solution, indicating that the presence of CaO in a geopolymer composite

491 results in the synthesis of CSH and Ca (OH)₂. A vigorous solution can quickly breakdown these
492 calcium-based hydrated products. Moreover, Hafez et. al [50], stated that the alkali-activated-
493 based mortar having 50% fly ash, 35% GGBS, and 15% silica fume demonstrated greater
494 resistance to magnesium sulphate than mortar containing 100% fly ash. The inclusion of WBA
495 and WGA dramatically enhanced the composites acid attack resistance and proved their
496 compatibility with the acid environment medium.

497 **3.2.4. Water absorption assessment**

498 Within the initial 8 hours, the water absorption rates of all composites showed a distinct
499 upward trend, followed by a stabilisation of the water absorption rate for all the composites
500 (see **Fig.11**). This pattern aligns, to some extent, with the ASTM C1585[51] standard, although
501 it's important to note that these composites are not OPC-based. The standard outlines two
502 phases of capillary absorption: the primary phase occurring between the initial measurement
503 and the one at 6 hours, and the secondary phase spanning from the first measurement to the
504 seventh day[52]. 70B and 100B samples had the highest water absorption rate, while the 50G
505 sample had the lowest (see **Fig. 11**). At the 96-hour mark, the water absorption for 70B and
506 100B measured approximately 8%, while 50G showed a slightly lower rate at around 6%,
507 indicating an approximate 8% reduction in water absorption compared to the control. The
508 control, with the second-lowest water absorption rate, decreased to approximately 6.5%
509 after 96 hours. In comparison, 70B and 100B exhibited water absorption rates about 25%
510 higher than the control. Following 96h, the water absorption rates of 70G, 100G, and 50B
511 were, respectively, 6.6%, 6.7%, and 7%, showing increases of about 1.5%, 3%, and 8%, relative
512 to the control. The results indicated that samples produced using waste brick aggregates had
513 higher water absorption rates compared to samples prepared with geo-cement aggregates.
514 This is due to the porous nature of recycled brick aggregates [53]. It's important to highlight
515 that the laboratory testing of aggregates in this study revealed water absorption values of
516 approximately 9.8%, 8%, and 7.5% for WBA, sand, and WGA, respectively. The water
517 absorption pattern observed in the incorporated composites mirrored that of the aggregates.
518 Nonetheless, the variances in water absorption rates among the composites were
519 comparable. Tavakoli et al. [18] reported that, in OPC-based composites, the amount of water
520 that concrete can hold is equal to the sum of how much water cement paste and aggregates
521 can hold. Since brick aggregates soak up more water than natural aggregates, this rise in water
522 absorption was expected, which is in line with observations made in this work. Furthermore,

523 Kasinikota et al. [54] validated the conclusions of this study by noting that the water
 524 absorption of samples based on Ordinary Portland Cement (OPC) rises with the increasing
 525 content of crushed brick waste, ranging from 8% to 11% as the dosage of crushed brick waste
 526 increases from 0% to 24%. Moreover, the percentage of brick powder in a gypsum-lime
 527 mortar increases the water absorption rate. Owing to the evaporation of the pooled water,
 528 the sample's porosity rises [55]. Priyanka et.al [56] reported that, the water absorption values
 529 were lower when the GGBS-base geopolymer aggregate replacement level was raised. As with
 530 time, GGBS's pozzolanic activity builds up. This means that there are fewer connections
 531 between voids, which makes it harder for water to get in. With an average particle size of 9.2
 532 μm , GGBS particles fill all holes and small cracks, making concrete with fewer pores. A high
 533 GGBS surface area helps limit the aggregates' water absorption [40]. This finding explains why
 534 50G had the lowest water absorption rate as it had better interlocking bond and less voids
 535 compared to 70G and 100G achieved higher water absorption rates. Further study is required
 536 to understand more about the microstructure of composites, as there is currently a scarcity
 537 of data on this topic. Yet, the fluctuations in water absorption rates of the mortar composites
 538 incorporated with WBA and WGA were tolerable. According to G. Golewski [57], water
 539 absorption of concrete below 10% is already deemed minimal. The inclusion of WBA and WGA
 540 into AAM composites has intriguing effects in terms of water absorption.



541
 542 **Figure 11.** Water absorption of AAM with waste brick and geo-cement aggregates at
 543 different replacement ratios

544 **4. Conclusions**

545 The study focused on evaluating a versatile strategy for emission reduction in the global
 546 cement and concrete industries, utilising alkali-activation for low-carbon cement and

547 incorporating waste-derived aggregates from bricks and geo-cement. Aiming to contribute to
548 eco-sustainability in construction, the research assesses the engineering potential of these
549 waste aggregates by analysing microstructure, mechanical performance, and durability
550 properties, emphasising their substitution for virgin raw materials.

- 551 1. Specimens incorporating brick and geo-cement aggregates demonstrated mechanical
552 performance, including flexural and compressive strengths, which either exceeded or
553 were comparable to specimens with natural aggregates across all replacement ratios.
- 554 2. The surface roughness texture and angularity of brick and geo-cement aggregates
555 exhibited compatibility, resulting in enhanced bonding with the matrix paste. Notably, the
556 50B and 70G samples showcased superior compressive (61 MPa) and flexural (12 MPa)
557 strengths.
- 558 3. Incorporation of both brick and geo-cement aggregates in Alkali-Activated Materials
559 (AAMs) exhibited enhanced resistance to acid attacks. Specifically, 100B and 100G
560 showed minimal compressive strength losses of 2.5% and 8%, respectively, following an
561 acid attack.
- 562 4. Among the evaluated mixes, 50G demonstrated the lowest water absorption rate and
563 post-freeze-thaw compressive strength loss, registering values of 6% and 13%,
564 respectively.
- 565 5. In the chloride attack test, 100B and 70B displayed the most favourable post-compressive
566 strength losses at 13% and 18%, respectively.

567 Upon comprehensive analysis of the overall performance results across various tests, the
568 recommended mixture is 50B, followed by 50G. Specifically, 50B exhibited a compressive
569 strength of 61 MPa, flexural strength of 11 MPa, 26% weight loss after the chloride test, a 7%
570 water absorption rate, and after the acid test, a 24% compressive strength loss and 1.6%
571 weight loss. Furthermore, following freeze-thaw cycles, 50B displayed a 17% compressive
572 strength loss and a 2.2% weight loss. Given the superior overall performance achieved with a
573 50% replacement of both brick and geo-cement aggregates in Alkali-Activated Materials
574 (AAM) composites, future investigations should focus on increasing the replacement ratio of
575 waste aggregates while ensuring the maintenance of sufficient properties by either applying
576 pretreatment to the aggregates or adding additives to the mix. Additionally, comprehensive
577 assessments are necessary, considering the economic and environmental implications of
578 incorporating waste aggregates into cementitious composites, along with technical and

579 performance considerations. A rigorous evaluation of the economic feasibility of this study is
580 imperative to gauge its potential for large-scale deployment and commercialisation.

581 **Acknowledgement**

582 This work was funded as part of the DigiMat project, which has received funding from the
583 European Union's Horizon 2020 research and innovation program under the Marie
584 Skłodowska-Curie grant agreement ID: 101029471.

585 **References**

- 586 [1] J. Kirchherr, D. Reike, M. Hekkert, Conceptualizing the circular economy: An analysis
587 of 114 definitions, *Resour. Conserv. Recycl.* 127 (2017) 221–232.
588 <https://doi.org/10.1016/j.resconrec.2017.09.005>.
- 589 [2] K.Y.G. Kwok, J. Kim, A.M. Asce, W.K.O. Chong, M. Asce, S.T. Ariaratnam, F. Asce,
590 Structuring a Comprehensive Carbon-Emission Framework for the Whole Lifecycle of
591 Building, Operation, and Construction, (2016).
592 [https://doi.org/10.1061/\(ASCE\)AE.1943-5568.0000215](https://doi.org/10.1061/(ASCE)AE.1943-5568.0000215).
- 593 [3] E. Benhelal, E. Shamsaei, M.I. Rashid, Challenges against CO2 abatement strategies in
594 cement industry: A review, *J. Environ. Sci. (China)*. 104 (2021) 84–101.
595 <https://doi.org/10.1016/j.jes.2020.11.020>.
- 596 [4] L. Proaño, A.T. Sarmiento, M. Figueredo, M. Cobo, Techno-economic evaluation of
597 indirect carbonation for CO2 emissions capture in cement industry: A system
598 dynamics approach, *J. Clean. Prod.* 263 (2020).
599 <https://doi.org/10.1016/j.jclepro.2020.121457>.
- 600 [5] J.L. Provis, S.A. Bernal, Geopolymers and related alkali-activated materials, *Annu. Rev.*
601 *Mater. Res.* 44 (2014) 299–327. [https://doi.org/10.1146/annurev-matsci-070813-](https://doi.org/10.1146/annurev-matsci-070813-113515)
602 [113515](https://doi.org/10.1146/annurev-matsci-070813-113515).
- 603 [6] S.A. Bernal, J.L. Provis, Durability of alkali-activated materials: Progress and
604 perspectives, *J. Am. Ceram. Soc.* 97 (2014) 997–1008.
605 <https://doi.org/10.1111/jace.12831>.
- 606 [7] Y. Zhang, W. Luo, J. Wang, Y. Wang, Y. Xu, J. Xiao, A review of life cycle assessment of
607 recycled aggregate concrete, *Constr. Build. Mater.* 209 (2019) 115–125.
608 <https://doi.org/10.1016/j.conbuildmat.2019.03.078>.
- 609 [8] J. Shi, J. Tan, B. Liu, J. Chen, J. Dai, Z. He, Experimental study on full-volume slag alkali-
610 activated mortars: Air-cooled blast furnace slag versus machine-made sand as fine
611 aggregates, *J. Hazard. Mater.* 403 (2021) 123983.
612 <https://doi.org/10.1016/j.jhazmat.2020.123983>.
- 613 [9] B.C. Mendes, L.G. Pedroti, C.M.F. Vieira, M. Marvila, A.R.G. Azevedo, J.M. Franco de
614 Carvalho, J.C.L. Ribeiro, Application of eco-friendly alternative activators in alkali-
615 activated materials: A review, *J. Build. Eng.* 35 (2021).
616 <https://doi.org/10.1016/j.jobbe.2020.102010>.
- 617 [10] I. Almeshal, B.A. Tayeh, R. Alyousef, H. Alabduljabbar, A. Mustafa Mohamed, A.

- 618 Alaskar, Use of recycled plastic as fine aggregate in cementitious composites: A
619 review, *Constr. Build. Mater.* 253 (2020) 119146.
620 <https://doi.org/10.1016/j.conbuildmat.2020.119146>.
- 621 [11] K. Kabirifar, M. Mojtahedi, C. Wang, V.W.Y. Tam, Construction and demolition waste
622 management contributing factors coupled with reduce, reuse, and recycle strategies
623 for effective waste management: A review, *J. Clean. Prod.* 263 (2020) 121265.
624 <https://doi.org/10.1016/j.jclepro.2020.121265>.
- 625 [12] H. Ilcan, O. Sahin, A. Kul, E. Ozcelikci, M. Sahmaran, Rheological property and
626 extrudability performance assessment of construction and demolition waste-based
627 geopolymer mortars with varied testing protocols, *Cem. Concr. Compos.* 136 (2023)
628 104891. <https://doi.org/10.1016/J.CEMCONCOMP.2022.104891>.
- 629 [13] C.L. Wong, K.H. Mo, S.P. Yap, U.J. Alengaram, T.C. Ling, Potential use of brick waste as
630 alternate concrete-making materials: A review, *J. Clean. Prod.* 195 (2018) 226–239.
631 <https://doi.org/10.1016/j.jclepro.2018.05.193>.
- 632 [14] K. Rashid, E.U. Haq, M.S. Kamran, N. Munir, A. Shahid, I. Hanif, Experimental and
633 finite element analysis on thermal conductivity of burnt clay bricks reinforced with
634 fibers, *Constr. Build. Mater.* 221 (2019) 190–199.
635 <https://doi.org/10.1016/J.CONBUILDMAT.2019.06.055>.
- 636 [15] Z. He, A. Shen, H. Wu, W. Wang, L. Wang, C. Yao, J. Wu, Research progress on
637 recycled clay brick waste as an alternative to cement for sustainable construction
638 materials, *Constr. Build. Mater.* 274 (2021) 122113.
639 <https://doi.org/10.1016/j.conbuildmat.2020.122113>.
- 640 [16] M. Ngoc-Tra Lam, D.-H. Le, D.-L. Nguyen, Reuse of clay brick and ceramic waste in
641 concrete: A study on compressive strength and durability using the Taguchi and Box–
642 Behnken design method, *Constr. Build. Mater.* 373 (2023) 130801.
643 <https://doi.org/10.1016/j.conbuildmat.2023.130801>.
- 644 [17] S. Mesgari, A. Akbarnezhad, J.Z. Xiao, Recycled geopolymer aggregates as coarse
645 aggregates for Portland cement concrete and geopolymer concrete: Effects on
646 mechanical properties, *Constr. Build. Mater.* 236 (2020) 117571.
647 <https://doi.org/10.1016/j.conbuildmat.2019.117571>.
- 648 [18] D. Tavakoli, P. Fakharian, J. de Brito, Mechanical properties of roller-compacted
649 concrete pavement containing recycled brick aggregates and silica fume, *Road Mater.*
650 *Pavement Des.* 23 (2022) 1793–1814.
651 <https://doi.org/10.1080/14680629.2021.1924236>.
- 652 [19] M.M. Atyia, M.G. Mahdy, M. Abd Elrahman, Production and properties of lightweight
653 concrete incorporating recycled waste crushed clay bricks, *Constr. Build. Mater.* 304
654 (2021) 124655. <https://doi.org/10.1016/j.conbuildmat.2021.124655>.
- 655 [20] C. Wang, J. Xiao, W. Liu, Z. Ma, Unloading and reloading stress-strain relationship of
656 recycled aggregate concrete reinforced with steel/polypropylene fibers under uniaxial
657 low-cycle loadings, *Cem. Concr. Compos.* 131 (2022) 104597.
658 <https://doi.org/10.1016/J.CEMCONCOMP.2022.104597>.

- 659 [21] C. Wang, H. Wu, C. Li, Hysteresis and damping properties of steel and polypropylene
660 fiber reinforced recycled aggregate concrete under uniaxial low-cycle loadings,
661 *Constr. Build. Mater.* 319 (2022) 126191.
662 <https://doi.org/10.1016/J.CONBUILDMAT.2021.126191>.
- 663 [22] C. Wang, J. Xiao, C. Qi, C. Li, Rate sensitivity analysis of structural behaviors of
664 recycled aggregate concrete frame, *J. Build. Eng.* 45 (2022) 103634.
665 <https://doi.org/10.1016/J.JOBE.2021.103634>.
- 666 [23] E. El-Seidy, M. Sambucci, M. Chougan, M.J. Al-Kheetan, I. Biblioteca, M. Valente, S.H.
667 Ghaffar, Mechanical and physical characteristics of alkali- activated mortars
668 incorporated with recycled polyvinyl chloride and rubber aggregates, *J. Build. Eng.* 60
669 (2022) 105043. <https://doi.org/10.1016/j.jobbe.2022.105043>.
- 670 [24] E. El-Seidy, M. Chougan, M. Sambucci, M.J. Al-Kheetan, I. Biblioteca, M. Valente, S.
671 Hamidreza Ghaffar, Lightweight alkali-activated materials and ordinary Portland
672 cement composites using recycled polyvinyl chloride and waste glass aggregates to
673 fully replace natural sand, (2023).
674 <https://doi.org/10.1016/j.conbuildmat.2023.130399>.
- 675 [25] B. Panda, M.J. Tan, Rheological behavior of high volume fly ash mixtures containing
676 micro silica for digital construction application, *Mater. Lett.* 237 (2019) 348–351.
677 <https://doi.org/10.1016/j.matlet.2018.11.131>.
- 678 [26] M. Chougan, S. Hamidreza Ghaffar, M. Jahanzat, A. Albar, N. Mujaddedi, R. Swash,
679 The influence of nano-additives in strengthening mechanical performance of 3D
680 printed multi-binder geopolymer composites, (n.d.).
681 <https://doi.org/10.1016/j.conbuildmat.2020.118928>.
- 682 [27] E. El-seidy, M. Sambucci, M. Chougan, Y.A. Ai-noaimat, M.J. Al-kheetan, I. Biblioteca,
683 M. Valente, S. Hamidreza, Alkali activated materials with recycled unplasticised
684 polyvinyl chloride aggregates for sand replacement, *Constr. Build. Mater.* 409 (2023)
685 134188. <https://doi.org/10.1016/j.conbuildmat.2023.134188>.
- 686 [28] M. Moranville, S. Kamali, E. Guillon, Physicochemical equilibria of cement-based
687 materials in aggressive environments—experiment and modeling, *Cem. Concr. Res.*
688 34 (2004) 1569–1578.
- 689 [29] B.S. EN, 1097-6. Tests for mechanical and physical properties of aggregates, *Determ.*
690 *Part. Density Water Absorption*, BSI. (2013).
- 691 [30] P. Zhu, M. Hua, H. Liu, X. Wang, C. Chen, Interfacial evaluation of geopolymer mortar
692 prepared with recycled geopolymer fine aggregates, *Constr. Build. Mater.* 259 (2020)
693 119849. <https://doi.org/10.1016/j.conbuildmat.2020.119849>.
- 694 [31] G. Santha Kumar, Influence of fluidity on mechanical and permeation performances
695 of recycled aggregate mortar, *Constr. Build. Mater.* 213 (2019) 404–412.
696 <https://doi.org/10.1016/j.conbuildmat.2019.04.093>.
- 697 [32] S. Iftikhar, K. Rashid, E. Ul Haq, I. Zafar, F.K. Alqahtani, M. Iqbal Khan, Synthesis and
698 characterization of sustainable geopolymer green clay bricks: An alternative to burnt
699 clay brick, *Constr. Build. Mater.* 259 (2020) 119659.

- 700 <https://doi.org/10.1016/J.CONBUILDMAT.2020.119659>.
- 701 [33] M. Khattab, S. Hachemi, M. Fawzi, A. Ajlouni, The Use of Recycled Aggregate From
702 Waste Refractory Brick For The Future Of Sustainable Concrete, *Int. Congr.*
703 *Phenomenol. Asp. Civ. Eng.* (2021) 1–6.
- 704 [34] O.M. Olofinnade, J.I. Ogara, I.T. Oyawoye, A.N. Ede, J.M. Ndambuki, K.D. Oyeyemi,
705 D.O. Nduka, Mechanical properties of high strength eco-concrete containing crushed
706 waste clay brick aggregates as replacement for sand, *IOP Conf. Ser. Mater. Sci. Eng.*
707 640 (2019). <https://doi.org/10.1088/1757-899X/640/1/012046>.
- 708 [35] F.S. Klak, H. Saleh, A.S. Tais, Recycling of crushed clay bricks as fine aggregate in
709 concrete and cement mortar, *Aust. J. Struct. Eng.* 00 (2022) 1–10.
710 <https://doi.org/10.1080/13287982.2022.2098600>.
- 711 [36] P. Shewale, P. Thorat, A. Bagat, A. Patil, R. Khaware, M. Kamble, S.B. Pawar,
712 Experimental Study on Assessment of Fly Ash and GGBS Based Geopolymer Mortar
713 with Brick Waste Replacement to Fine Aggregates, *Int. Res. J. Eng. Technol.* (2022)
714 1392–1398. www.irjet.net.
- 715 [37] W.I. Khalil, Q.J. Frayyeh, M.F. Ahmed, Evaluation of sustainable metakaolin-
716 geopolymer concrete with crushed waste clay brick, *IOP Conf. Ser. Mater. Sci. Eng.*
717 518 (2019). <https://doi.org/10.1088/1757-899X/518/2/022053>.
- 718 [38] R. Wang, Z. Hu, Y. Li, K. Wang, H. Zhang, Review on the deterioration and approaches
719 to enhance the durability of concrete in the freeze–thaw environment, *Constr. Build.*
720 *Mater.* 321 (2022) 126371. <https://doi.org/10.1016/j.conbuildmat.2022.126371>.
- 721 [39] L. Reig, M.M. Tashima, M. V. Borrachero, J. Monzó, C.R. Cheeseman, J. Payá,
722 Properties and microstructure of alkali-activated red clay brick waste, *Constr. Build.*
723 *Mater.* 43 (2013) 98–106. <https://doi.org/10.1016/j.conbuildmat.2013.01.031>.
- 724 [40] J. Zhao, L. Tong, B. Li, T. Chen, C. Wang, G. Yang, Y. Zheng, Eco-friendly geopolymer
725 materials: A review of performance improvement, potential application and
726 sustainability assessment, *J. Clean. Prod.* 307 (2021) 127085.
727 <https://doi.org/10.1016/J.JCLEPRO.2021.127085>.
- 728 [41] I. Ismail, S.A. Bernal, J.L. Provis, R. San Nicolas, D.G. Brice, A.R. Kilcullen, S. Hamdan,
729 J.S.J. Van Deventer, Influence of fly ash on the water and chloride permeability of
730 alkali-activated slag mortars and concretes, *Constr. Build. Mater.* 48 (2013) 1187–
731 1201. <https://doi.org/10.1016/j.conbuildmat.2013.07.106>.
- 732 [42] M.H. Tadayon, M. Shekarchi, M. Tadayon, Long-term field study of chloride ingress in
733 concretes containing pozzolans exposed to severe marine tidal zone, *Constr. Build.*
734 *Mater.* 123 (2016) 611–616. <https://doi.org/10.1016/j.conbuildmat.2016.07.074>.
- 735 [43] R. Vedalakshmi, K. Rajagopal, N. Palaniswamy, Longterm corrosion performance of
736 rebar embedded in blended cement concrete under macro cell corrosion condition,
737 *Constr. Build. Mater.* 22 (2008) 186–199.
738 <https://doi.org/10.1016/j.conbuildmat.2006.09.004>.
- 739 [44] X. Shi, N. Xie, K. Fortune, J. Gong, Durability of steel reinforced concrete in chloride
740 environments: An overview, *Constr. Build. Mater.* 30 (2012) 125–138.

- 741 <https://doi.org/10.1016/j.conbuildmat.2011.12.038>.
- 742 [45] K. Samimi, S. Kamali-Bernard, A. Akbar Maghsoudi, M. Maghsoudi, H. Siad, Influence
743 of pumice and zeolite on compressive strength, transport properties and resistance to
744 chloride penetration of high strength self-compacting concretes, *Constr. Build. Mater.*
745 151 (2017) 292–311. <https://doi.org/10.1016/j.conbuildmat.2017.06.071>.
- 746 [46] H. Janfeshan Araghi, I.M. Nikbin, S. Rahimi Reskati, E. Rahmani, H. Allahyari, An
747 experimental investigation on the erosion resistance of concrete containing various
748 PET particles percentages against sulfuric acid attack, *Constr. Build. Mater.* 77 (2015)
749 461–471. <https://doi.org/10.1016/j.conbuildmat.2014.12.037>.
- 750 [47] A.M. Izzat, A.M.M. Al Bakri, H. Kamarudin, L.M. Moga, G.C.M. Ruzaidi, M.T.M.
751 Faheem, A.V. Sandu, Microstructural analysis of geopolymer and ordinary Portland
752 cement mortar exposed to sulfuric acid, *Mater. Plast.* 50 (2013) 171–174.
- 753 [48] M. Vafaei, A. Allahverdi, P. Dong, N. Bassim, M. Mahinroosta, Resistance of red clay
754 brick waste/phosphorus slag-based geopolymer mortar to acid solutions of mild
755 concentration, *J. Build. Eng.* 34 (2021) 102066.
756 <https://doi.org/10.1016/j.jobe.2020.102066>.
- 757 [49] P. Nuaklong, A. Wongsas, V. Sata, K. Boonserm, J. Sanjayan, Heliyon Properties of high-
758 calcium and low-calcium fly ash combination geopolymer mortar containing recycled
759 aggregate, *Heliyon.* 5 (2019) e02513. <https://doi.org/10.1016/j.heliyon.2019.e02513>.
- 760 [50] H.E. Elyamany, A. Elmoaty, M.A. Elmoaty, A. Rahman, Sulphuric Acid Resistance of
761 Slag Geopolymer Concrete Modified with Fly Ash and Silica Fume, *Iran. J. Sci. Technol.*
762 *Trans. Civ. Eng.* 45 (2021) 2297–2315. <https://doi.org/10.1007/s40996-020-00515-5>.
- 763 [51] ASTM-C1585 | Standard Test Method for Measurement of Rate of Absorption of
764 Water by Hydraulic-Cement Concretes | Document Center, Inc., (n.d.).
765 <https://www.document-center.com/standards/show/ASTM-C1585> (accessed
766 December 16, 2023).
- 767 [52] M. Frías, M. Monasterio, J. Moreno-Juez, Physical and Mechanical Behavior of New
768 Ternary and Hybrid Eco-Cements Made from Construction and Demolition Waste,
769 *Materials (Basel).* 16 (2023). <https://doi.org/10.3390/ma16083093>.
- 770 [53] B. Debnath, P. Pratim Sarkar, Quantification of random pore features of porous
771 concrete mixes prepared with brick aggregate: An application of stereology and
772 mathematical morphology, *Constr. Build. Mater.* 294 (2021) 123594.
773 <https://doi.org/10.1016/j.conbuildmat.2021.123594>.
- 774 [54] P. Kasinikota, D.D. Tripura, Evaluation of compressed stabilized earth block properties
775 using crushed brick waste, *Constr. Build. Mater.* 280 (2021) 122520.
776 <https://doi.org/10.1016/j.conbuildmat.2021.122520>.
- 777 [55] K. Naciri, I. Aalil, A. Chaaba, Eco-friendly gypsum-lime mortar with the incorporation
778 of recycled waste brick, *Constr. Build. Mater.* 325 (2022) 126770.
779 <https://doi.org/10.1016/j.conbuildmat.2022.126770>.
- 780 [56] M. Priyanka, K. Muniraj, S.R.C. Madduru, Influence of geopolymer aggregates on
781 micro-structural and durability characteristics of OPC concrete, *J. Build. Pathol.*

- 782 Rehabil. 7 (2022) 1–16. <https://doi.org/10.1007/s41024-021-00153-y>.
- 783 [57] G.L. Golewski, Assessing of water absorption on concrete composites containing fly
784 ash up to 30 % in regards to structures completely immersed in water, Case Stud.
785 Constr. Mater. 19 (2023) e02337. <https://doi.org/10.1016/J.CSCM.2023.E02337>.
- 786

Journal Pre-proof

Declaration of interests

The authors declare that they have no known competing financial interests or personal relationships that could have appeared to influence the work reported in this paper.

The authors declare the following financial interests/personal relationships which may be considered as potential competing interests:

Journal Pre-proof